



# Constraining titanium tartrate in the interlayer space of layered double hydroxides induces enantioselectivity

Huimin Shi, Chenguang Yu, Jing He \*

State Key Laboratory of Chemical Resource Engineering, Beijing University of Chemical Technology, Beijing 100029, China

## ARTICLE INFO

### Article history:

Received 22 December 2009

Revised 30 January 2010

Accepted 2 February 2010

Available online 5 March 2010

### Keywords:

Layered double hydroxides

Titanium tartrate complex

Enantioselectivity

Sulfoxidation

Confinement effect

## ABSTRACT

Kagan-Medona and Sharpless titanium tartrate complexes (Ti(IV)TA<sub>m</sub>, subscript m represents the coordination ratio of L-tartaric acid to the Ti center in the complex) have been intercalated into the interlayer of layered double hydroxides (LDHs) by anionic exchange method using Mg/Al-CO<sub>3</sub> LDH as the precursor. Titanium tartrate-intercalated LDHs (designated Mg/Al-Ti(IV)TA<sub>m</sub> LDHs) with varied interlayer spacing were produced by tuning the area unit charge (*A<sub>c</sub>*) of the brucite-like layer from 0.24 to 0.44 nm<sup>2</sup>. The interlayer spacing decreases from 1.87 to 1.44 nm with the increase in *A<sub>c</sub>*. The interlayer titanium tartrate anions are present in an interdigitated bilayer arrangement. The bidimensional interlayer space can be swollen, and thus accommodates the reactants in the interlayer. The titanium tartrate complex constrained in the LDH interlayer region shows enhanced asymmetric induction in the heterogeneous sulfoxidation of pro-chiral methyl phenyl sulfide.

© 2010 Elsevier Inc. All rights reserved.

## 1. Introduction

With intense striving for environmentally benign chemical processes or methodologies, much attention [1–3] has been paid on the immobilization of homogeneous catalytic sites. The heterogeneous catalysts retain the active sites of homogeneous analogues and facilitate perfect separation and subsequent recycle. Titanium tartrate complexes [4] are well known as selective oxidation homogeneous catalysts, and their immobilization has been reported. An early attempt was made by Farrell et al. [5], who developed a polymer-supported soluble system by binding a single tartrate ester unit to a polystyrene resin. A modest chiral induction (ca. 50–60% ee) in the epoxidation of allylic alcohols was achieved under the same reaction conditions as in the Sharpless reaction. No homogeneous result was reported as a control, but all the ee values were lower than 90% of that in Sharpless system. A group of insoluble linear poly (tartrate ester)s were later employed as ligands to Ti(OPr<sup>i</sup>)<sub>4</sub> by Canali et al. [6]. The enantiomer excess in the epoxidation of trans-hex-2-en-1-ol was found to vary in the range of 41–79%, lower than the observed for the homogeneous analogue in all cases. Owing to the swelling of gel-type polymers in the catalytic reactions, inorganic supports have been developed with their good chemical, mechanical and thermal stabilities. Choudary et al. [7] reported the first intercalation of Ti<sup>4+</sup> using tartrate ester as ligand in montmorillonite. In the asymmetric epoxidation of allylic alcohols, the titanium centers intercalated in the interlayer galler-

ies of montmorillonite host, in the presence of chiral tartrate ester, gave an enantiomer excess comparable to that achieved by homogeneous Ti(OPr<sup>i</sup>)<sub>4</sub> and dimethyl tartrate. Xiang et al. [8] reported the preparation of organic–inorganic hybrid materials by grafting a chiral tartaric acid derivative on the silica surface and in the mesopores of MCM-41. The enantioselectivities in the heterogeneous system was as good as that in the homogeneous analogue in the epoxidation of allyl alcohol.

Recently, new opportunities have emerged for the heterogenization of metal complex catalyst, i.e. the enantioselectivity was possible to be enhanced by controlling the reaction process in mesoscale or microscale using the cooperativity of solid surfaces [9] and the confinement effects in a constricted system [10,11]. The confinement effects in the pores or channels of zeolites [12] and mesoporous silica materials [13,14] have been well revealed. Significant improvement in catalytic performances (activity, stability and enantioselectivity) has been achieved [15–20] by confining the catalytic sites in the ‘rigid’ nano-sized pores of mesoporous supports. Constraining [Co(salen)] complexes in the nanocages of SBA-16 improved the conversion and ee in the hydrolytic kinetic resolution of epoxides [15]. The enantioselectivity, for example, was boosted by reducing the pore size of silica from 250 to 60 Å and further 38 Å in the asymmetric hydrogenation of methyl benzoylformate using rhodium and palladium complexes. The enhancement of enantioselectivity logically reflected the increasing influence of spatial constraint [16]. Therefore, the enantioselectivity enhancement was contributed to the predisposed access of reactant to catalytic center by the spatial constraint of the walls of rigid pores [16] or the restricted access of pro-chiral reactant to the active center generated

\* Corresponding author. Fax: +86 10 6442 5385.

E-mail address: [jinghe@263.net.cn](mailto:jinghe@263.net.cn) (J. He).

by the pore concavity and curvature [17]. Even non-enantioselective catalysts showed significant asymmetric induction when anchored into 'rigid' confining nanospaces [21,22].

Different from zeolites and mesoporous materials, layered double hydroxides (LDHs), a class of layer-structured materials with tailorable interlayer galleries [23], provides 'flexible' confining spaces. The confining space could be adjusted by changing the size and arrangement of guest molecules [24–26]. The flexible interlayer spaces not only can fit small-sized moieties but also are capable of accommodating bulky catalytic sites. The bulky catalytic sites are difficult or even impossible to enter the rigid pores with fixed dimension. Additional attraction for the LDH supports is the non-covalent interaction between the intercalated catalytic moieties and host layers, which avoids the modification of chiral ligand required by its covalent binding to support surface. The salen–Mn (III) complex, which was intercalated into Zn/Al-LDHs, displayed higher conversion, chemical selectivity and diastereoselectivity than the analogues occluded in X and Y zeolites via the "ship-in-bottle" approach in the stereoselective epoxidation of R-(+)-limonene using molecular oxygen [27]. The  $\text{OsO}_4^{2-}$ , though immobilized just on LDH surface [28], showed higher activity and enantioselectivity than the Kobayashi catalyst in the asymmetric dihydroxylation of olefins using 1,4-bis(9-O-dihydroquinidiny)phthalazine as chiral ligand. Iron (III)–porphyrin complexes were intercalated into Zn/Al-LDHs and used as catalysts in the oxidation of cyclooctene, cyclohexene, and cyclohexane with iodosylbenzene as oxidant [29]. The catalytic activity of heterogeneous iron (III)–porphyrins catalyst was found to depend on the chemical environments of iron (III)–porphyrins. The synergistic effects of LDH layers with the supported nanopalladium have also been proposed, in which the LDH layers acted as basic ligands [30]. But the confinement effects related with the tunable bidimensional space have never been discussed in detail.

In this work, LDHs were employed to support the titanium tartrate complex (designated  $\text{Ti(IV)TA}_m$ , subscript  $m$  represents the coordination ratio of L-tartaric acid ligand to Ti center in the titanium tartrate complex) through simple ion-exchange approach. The interlayer spacing of  $\text{Ti(IV)TA}_2$  intercalated LDHs was rationally tuned through tailoring the area unit charge ( $A_c$ ) of LDH layers, and the consequent confinement effects in the bidimensional space were investigated. The confinement was found to predispose stereo-selectivity and enhanced enantioselectivity was achieved.

## 2. Experimental

### 2.1. Materials

L-Tartaric acid (Aldrich, 99.5%),  $\text{Ti(OPr}^i)_4$  (Aldrich, 97%), methyl phenyl sulfide (Acros, 99%), methyl phenyl sulfoxide (Aldrich, 97%), and  $\text{H}_2\text{O}_2$  (30% aqueous solution) were used as received without further purification.  $\text{Mg(NO}_3)_2 \cdot 6\text{H}_2\text{O}$ ,  $\text{Al(NO}_3)_3 \cdot 9\text{H}_2\text{O}$ , NaOH, anhydrous  $\text{Na}_2\text{CO}_3$ , *n*-butanol,  $\text{CH}_2\text{Cl}_2$ ,  $\text{CH}_3\text{OH}$ ,  $\text{CH}_3\text{CN}$ , and *N,N*-dimethyl formamide (DMF) are all of analytical purity. If necessary, *n*-butanol was first desiccated with anhydrous  $\text{MgSO}_4$  for 24 h and then distilled prior to use.  $\text{CH}_2\text{Cl}_2$  was first treated in 4 Å zeolite overnight, and then distilled in  $\text{CaH}_2$  to extract the water.

### 2.2. Synthesis

Firstly, carbonate-intercalated LDHs ( $\text{Mg/Al-CO}_3$  LDHs) were prepared using separate nucleation and aging steps [31]. Typically, a solution of 0.18 mol of  $\text{Mg(NO}_3)_2 \cdot 6\text{H}_2\text{O}$  and 0.06 mol of  $\text{Al(NO}_3)_3 \cdot 9\text{H}_2\text{O}$  dissolved in 122 mL of deionized water ( $\text{Mg/Al} = 3/1$ ) was mixed with a solution of 0.38 mol of NaOH and 0.12 mol of  $\text{Na}_2\text{CO}_3$  dissolved in 122 mL of deionized water in a

colloid mill rotating at 3000 rpm. In 2 min, the resulting slurry was transferred to an autoclave for static crystallization at 373 K for 8 h. The input Mg/Al ratio varied from 3/1 to 2/1 or 4/1. The actual Mg/Al ratios in final products were determined by ICP technique as 2.98, 1.98, and 4.03. The concentration of the alkali solution was related to metal ion concentration in  $[\text{NaOH}] = 1.6 [\text{Mg}^{2+} + \text{Al}^{3+}]$  and  $[\text{CO}_3^{2-}] = 2.0 [\text{Al}^{3+}]$ . The final precipitate was filtered, washed thoroughly with deionized water, and dried at 353 K for 12 h.

Titanium tartrate-intercalated LDHs (designated  $\text{Mg/Al-Ti(IV)-TA}_m$  LDHs) were prepared by the ion-exchanged method. The titanium tartrate complex was first prepared by dissolving L-tartaric acid to Ti alkoxide solution in *n*-butanol. The input ratio of L-tartaric acid to Ti is determined according to the input ratio of Kagan-Medona or Sharpless titanium tartrate complex.  $m = 2$  when the input ratio of L-tartaric acid to Ti equals or exceeds the input ratio of the Kagan-Medona complex.  $m = 1$  when the ratio of L-tartaric acid to Ti equals the input ratio of the Sharpless complex.

Typically,  $\text{Ti(OPr}^i)_4$  (0.0016 mol, 0.4 mL) and L-tartaric acid (0.008 mol) in a molar ratio of Ti/tartaric acid = 1/6 was mixed in 50 mL of *n*-butanol and then refluxed for 1 h. LDHs- $\text{CO}_3$  as intercalated precursor was then introduced in a molar ratio of L-tartaric acid/carbonate = 5/1. After 8 h reflux, the resulting solid was centrifuged, washed with anhydrous ethanol, and dried under vacuum at 353 K for 12 h. Two approaches were taken to adjust the area unit charge of LDH layer. One is to change the initial chemical composition of LDH precursor by varying the Mg/Al input (as introduced in the synthesis of LDHs- $\text{CO}_3$ ), and the other is to input L-tartaric acid in different excesses in the synthesis of the  $\text{Ti(IV)TA}_2$  complex. The excess L-tartaric acid is used to modify the brucite-like layer composition in the carboxyl deprotonation and intercalation process, thereby fine-tuning the  $A_c$  value. Using  $\text{Mg}_{2.98}\text{Al-CO}_3$  LDHs as precursors, the ratio of Ti to L-tartaric acid was varied in 1/2, 1/6, 1/8, and 1/12.

To prepare pristine  $\text{Ti(IV)TA}_2$  complex, 10 mmol of L-tartaric acid and 5 mmol of  $\text{Ti(OBu}^n)_4$  were mixed in 50 mL of *n*-butanol under agitation. After 1 h reflux, the solvent was removed in rotary evaporator at 353 K under reduced pressure. The residue was kept under anhydrous atmosphere. The input ratio of L-tartaric acid to  $\text{Ti(OBu}^n)_4$  was decreased to 1/1 to prepare  $\text{Ti(IV)TA}$  complex.

### 2.3. Characterization

Powder X-ray diffraction (PXRD) patterns were taken on a Shimadzu XRD-6000 diffractometer using  $\text{Cu K}\alpha$  radiation, with a step size of  $0.02^\circ$  and scan speed of 5 deg/min. The ICP analysis was performed on a Shimadzu ICPS-7500 inductively coupled plasma emission spectrometer by dissolving the samples in dilute  $\text{HNO}_3$  and  $\text{H}_2\text{O}_2$  aqueous solution. The C and H element analysis was carried out on an Elementar Co. Vario El elemental analyzer. The Fourier transform infrared (FT-IR) spectra were recorded on a Bruker Vector 22 FT-IR spectrometer using standard KBr method at a resolution of  $4 \text{ cm}^{-1}$ .  $^{13}\text{C}$  CP/MAS NMR spectra were obtained with a Bruker AV300 NMR spectrometer at a resonance frequency of 75.47 MHz. The chemical shifts are referred relative to TMS. TEM images were taken on a JEOL 2011 microscope operated at 200 kV. The samples were prepared by dipping carbon-coated copper TEM grids with dilute ethanol suspension. CD spectra were recorded on a JASCO J-810 spectropolarimeter at room temperature in  $\text{CH}_3\text{CN}$  ( $c \approx 2 \times 10^{-5} \text{ M}$ ) in 1.0 mm cells. During the measurement, the instrument was thoroughly purged with  $\text{N}_2$ .

### 2.4. Sulfoxidation

Typically, the catalytic sulfoxidation was performed as follows. In a sealed 50 mL Erlenmeyer flask, methyl phenyl sulfide

(1.0 mmol), catalyst (equivalent to 0.050 mmol of  $\text{Ti}^{4+}$ ), and solvent (10 mL) were first bubbled with nitrogen gas, and then stirred for 1 h at room temperature and another 1 h at reaction temperature. The reaction was started by the addition of 30% aqueous  $\text{H}_2\text{O}_2$  as oxidant. The oxidant (in 10 mol% excess of methyl phenyl sulfide) was added slowly using a microliter syringe under vigorous stirring and with 10 s interruption between each drop. The reaction mixture was sampled at intervals. The sample was added with 0.03 g of  $\text{Na}_2\text{SO}_3$  to terminate the reaction, and then filtered using a 0.20  $\mu\text{m}$  microfilter. The filtrate was subject to Shimadzu HPLC with a Daicel chiral OB-H column (254 nm) for ee determination using *n*-hexane/*i*-propanol ( $v/v = 80/20$ ) as flow phase, and Shimadzu 2010 GC-MS instrument with a silicone capillary column (poly(5% diphenyl-95% dimethylsiloxane, 25 m  $\times$  0.2 mm, 0.33  $\mu\text{m}$  film thickness) for conversion and selectivity measurements.

### 3. Results and discussion

#### 3.1. Tuned interlayer spacing of $\text{Mg}/\text{Al}-\text{Ti}(\text{IV})\text{TA}_2$ LDHs

$\text{Ti}(\text{IV})\text{TA}_2$  was first intercalated into  $\text{Mg}_{2.98}\text{Al}-\text{CO}_3$  LDH through the ion-exchange approach with a constant input ratio of 5/1 of *L*-tartaric acid to Al. The ion-exchange is carried out in a non-aqueous medium to avoid  $\text{Ti}(\text{IV})$  hydrolysis and precipitation. The trace amount of water (less than 8 wt.%) physically absorbed on LDHs is used to facilitate the deprotonation of carboxylic groups of  $\text{Ti}(\text{IV})\text{TA}_2$  complex. To ensure the success of intercalation, butanol-*n* is rationally chosen as the intercalation medium because it is an efficient solvent for  $\text{Ti}(\text{IV})\text{TA}_2$  complex and has also been found to effectively swell the interlayer space [32].

In the ion-exchange of  $\text{Mg}_{2.98}\text{Al}-\text{CO}_3$  LDH with  $\text{Ti}(\text{IV})\text{TA}_2$ , the ratio of *L*-tartaric acid to Ti was firstly set as six. The ratio exceeds the stoichiometric ratio for the titanium tartrate coordination in Kagan-Medona structure. In the powder XRD pattern shown in Fig. 1, the reflections indexed [33] demonstrate a typical structure of LDHs with a hexagonal lattice in an  $R\bar{3}m$  rhombohedral symmetry. The (00*l*) reflections originating from the brucite-like layer

stacking obviously shift to lower  $2\theta$  angles, clearly revealing the successful ion-exchange of carbonate by  $\text{Ti}(\text{IV})\text{TA}_2$  complex anions. For  $\text{Mg}_{2.98}\text{Al}-\text{CO}_3$  LDH, the sharp and intense diffractions ascribed to (003) and (006) planes appear at  $2\theta = 11.5^\circ$  and  $22.5^\circ$ . The basal spacing calculated from (003) reflection is 0.77 nm, consistent with usually observed for  $\text{Mg}/\text{Al}$ -LDHs with carbonate as interlayer anions. For the ion-exchanged product, the (003) and (006) reflections shift to  $2\theta = 4.2^\circ$  and  $9.3^\circ$ . The basal spacing is increased to 2.09 nm. Subtracting the layer thickness (0.48 nm) from the basal spacing (2.09 nm), the interlayer spacing of  $\text{Mg}_{2.97}\text{Al}-\text{Ti}(\text{IV})\text{TA}_2$  LDH is estimated to be 1.61 nm. For  $\text{Mg}_{2.98}\text{Al}-\text{CO}_3$  LDH as intercalated precursor, the lattice parameter *a* ( $a = 2d_{(110)}$ ) is determined as 0.306 nm. The value of *a* corresponds to the distance between two metal cations and varies along with  $\text{M}(\text{II})/\text{M}(\text{III})$  ratio in the brucite-like layer ( $a = \sqrt{2}d_{(\text{M}-\text{O})}$ ). For the  $\text{Ti}(\text{IV})\text{TA}_2$  intercalated product with an input ratio of 6 of *L*-tartaric acid to Ti, *a* is estimated as 0.306 nm, corresponding to a  $\text{Mg}/\text{Al}$  ratio of 2.97. The area/unit charge ( $A_c$ ) in the brucite-like layer of  $\text{Mg}_{2.97}\text{Al}-\text{Ti}(\text{IV})\text{TA}_2$  LDH is calculated as  $0.32 \text{ nm}^2$  from  $A_c = (a^2 \sin 60^\circ)/x$ , where *x* equals to the ratio of  $\text{M}(\text{III})/[\text{M}(\text{II}) + \text{M}(\text{III})]$ . For  $\text{Mg}_{2.97}\text{Al}-\text{Ti}(\text{IV})\text{TA}_2$  LDH, *x* is 0.252.

It has been recognized that the interlayer spacing of LDHs depends on the charge density ( $1/A_c$ ) of brucite-like layer [34]. Herein,  $A_c$  is to be tailored by modifying the chemical composition of brucite-like layer with varied excess of *L*-tartaric acid, thereby tuning the interlayer spacing. The ratio of *L*-tartaric acid to Ti was varied from 6 to 2, 8 and 12. As shown in Fig. 1, the XRD reflections characteristic of  $\text{Mg}/\text{Al}-\text{Ti}(\text{IV})\text{TA}_2$  LDHs in each case were acquired. The resulting cell parameter *a*,  $A_c$ , and interlayer spacing were summarized in Table 1. When the input ratio of *L*-tartaric acid to Ti increases from 6 to 8, the metal composition of  $\text{Mg}/\text{Al}$  in the brucite-like layer is decreased from 2.97 to 2.30 (as shown in Table 1). The  $A_c$  decreases from 0.32 to  $0.27 \text{ nm}^2$ . The interlayer spacing of the  $\text{Mg}/\text{Al}-\text{Ti}(\text{IV})\text{TA}_2$  LDHs increases from 1.61 to 1.74 nm. However,  $A_c$  only slightly changes when the ratio of *L*-tartaric acid to Ti further rises to 12. No change in the interlayer spacing is thus observed. It appears unnecessary to input more *L*-tartaric acid. When the ratio of *L*-tartaric acid to Ti reduces to 2 (the exact stoichiometric ratio for Kagan-Medona coordination structure), the  $\text{Mg}/\text{Al}$  ratio in the brucite-like layer increases to 3.10, resulting in an  $A_c$  of  $0.33 \text{ nm}^2$ . The interlayer spacing of the  $\text{Mg}_{3.10}\text{Al}-\text{Ti}(\text{IV})\text{TA}_2$  LDHs is 1.60 nm, nearly the same as for the  $\text{Mg}_{2.97}\text{Al}-\text{Ti}(\text{IV})\text{TA}_2$  LDHs. It seems that, with a fixed brucite-like layer composition ( $\text{Mg}/\text{Al} = 2.98$  for example) of intercalated precursor, the interlayer spacing could be tuned only in a limited range by varying the excess input of *L*-tartaric acid. Hence, the brucite-like layer composition of the intercalated precursor was varied from 2.98 to 1.98 and 4.03. As shown in Table 1, when the  $\text{Mg}/\text{Al}$  ratio of intercalated precursor is decreased to 1.98, the  $A_c$  value reduces to  $0.24 \text{ nm}^2$ , and an interlayer spacing of 1.87 nm is produced. When the  $\text{Mg}/\text{Al}$  ratio of intercalated precursor is increased to 4.03, the  $A_c$  value rises to  $0.44 \text{ nm}^2$ , and an interlayer spacing of 1.52 nm is obtained. So in this work,  $A_c$  of  $\text{Mg}/\text{Al}-\text{Ti}(\text{IV})\text{TA}_2$  LDHs is tuned by varying both of the dosage of *L*-tartaric acid and the composition of brucite-like layer of  $\text{Mg}/\text{Al}-\text{CO}_3$  LDHs, thereby tuning the interlayer spacing. With the increase in  $A_c$ , the electrostatic attraction between the brucite-like layer and  $\text{Ti}(\text{IV})\text{TA}_2$  anions gets weakened. It can be seen clearly from Fig. 2 that the interlayer spacing decreases with the increase in  $A_c$ .

#### 3.2. Arrangement of $\text{Ti}(\text{IV})\text{TA}_2$ in the interlayer spaces

Fig. 3 illustrates TEM images of  $\text{Mg}_{2.97}\text{Al}-\text{Ti}(\text{IV})\text{TA}_2$  LDHs in bright (Fig. 3a and b) and dark (Fig. 3c and d) fields. The bright field TEM images show the approximately disk-like slabs. The same shapes are also revealed in the dark-field TEM images. From the

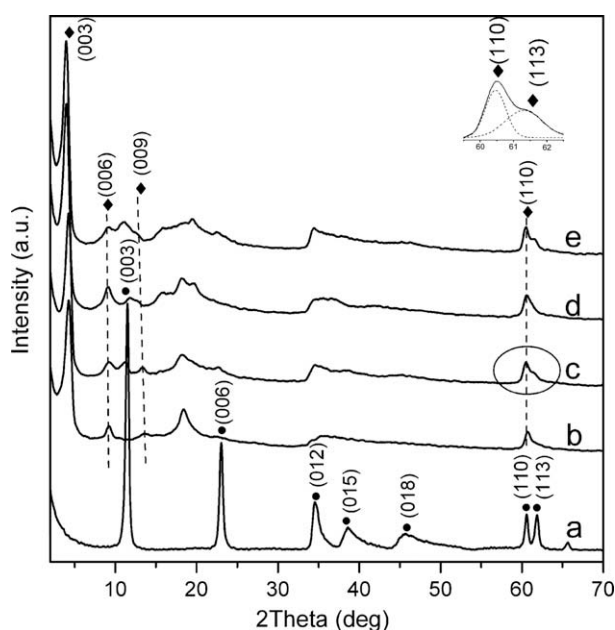


**Fig. 1.** XRD patterns of (a)  $\text{Mg}_{2.98}\text{Al}-\text{CO}_3$  LDH precursor and  $\text{Mg}/\text{Al}-\text{Ti}(\text{IV})\text{TA}_2$  LDH with input ratio of *L*-tartaric acid to Ti of (b) 2, (c) 6, (d) 8 and (e) 12. Inset: peak-fitting of (110) and (113) made by Origin 7.0 in Gaussian mode.

**Table 1**  
Chemical composition and structural parameters of Mg/Al–Ti(IV)TA<sub>2</sub> LDHs.

Precursor (M <sup>II</sup> /M <sup>III</sup> )	$a_p^a$ (nm)	Intercalates (M <sup>II</sup> /M <sup>III</sup> )	$a_i^b$ (nm)	$A_c$ (nm <sup>2</sup> )	$\iota$ -Tartaric acid/[Ti] in the solution	Interlayer spacing (nm)	Proposed formula according to the chemical composition <sup>c</sup>
4.03	0.307	4.37	0.307	0.44	6	1.52	$[\text{Mg}_{0.81}\text{Al}_{0.19}(\text{OH})_2]_2[(\text{Ti}(\text{IV})\text{TA}_2)_{0.03}^{2-}(\text{C}_4\text{H}_4\text{O}_6)_{0.03}^{2-}(\text{CO}_3)_{0.04}^{2-}]$
2.98	0.306	3.10	0.306	0.33	2	1.60	$[\text{Mg}_{0.76}\text{Al}_{0.24}(\text{OH})_2]_2[(\text{Ti}(\text{IV})\text{TA}_2)_{0.07}^{2-}(\text{C}_4\text{H}_4\text{O}_6)_{0.03}^{2-}(\text{CO}_3)_{0.02}^{2-}]$
		2.97	0.306	0.32	6	1.61	$[\text{Mg}_{0.75}\text{Al}_{0.25}(\text{OH})_2]_2[(\text{Ti}(\text{IV})\text{TA}_2)_{0.04}^{2-}(\text{C}_4\text{H}_4\text{O}_6)_{0.05}^{2-}(\text{CO}_3)_{0.03}^{2-}]$
		2.30	0.306	0.27	8	1.74	$[\text{Mg}_{0.70}\text{Al}_{0.30}(\text{OH})_2]_2[(\text{Ti}(\text{IV})\text{TA}_2)_{0.02}^{2-}(\text{C}_4\text{H}_4\text{O}_6)_{0.11}^{2-}(\text{CO}_3)_{0.02}^{2-}]$
		2.21	0.305	0.26	12	1.75	$[\text{Mg}_{0.69}\text{Al}_{0.31}(\text{OH})_2]_2[(\text{Ti}(\text{IV})\text{TA}_2)_{0.03}^{2-}(\text{C}_4\text{H}_4\text{O}_6)_{0.10}^{2-}(\text{CO}_3)_{0.02}^{2-}]$
1.98	0.305	1.94	0.305	0.24	6	1.87	$[\text{Mg}_{0.66}\text{Al}_{0.34}(\text{OH})_2]_2[(\text{Ti}(\text{IV})\text{TA}_2)_{0.03}^{2-}(\text{C}_4\text{H}_4\text{O}_6)_{0.14}^{2-}]$

<sup>a</sup>  $a_p$  is denoted as the cell parameter  $a$  of the precursor.

<sup>b</sup>  $a_i$  is denoted as the cell parameter  $a$  of Mg/Al–Ti(IV)TA<sub>2</sub> LDHs.

<sup>c</sup> Ti(IV)TA<sub>2</sub> is short for Kagan-Medona titanium tartrate complex, its molecular formula is  $[\text{Ti}_2(\text{C}_4\text{H}_4\text{O}_4)_2(\text{C}_4\text{H}_4\text{O}_6)_2(\text{OC}_4\text{H}_9)_2]$ .  $(\text{Ti}(\text{IV})\text{TA}_2)^{2-}$  represents  $[\text{Ti}_2(\text{C}_4\text{H}_4\text{O}_6)_4(\text{OC}_4\text{H}_9)_2]^{2-}$ .

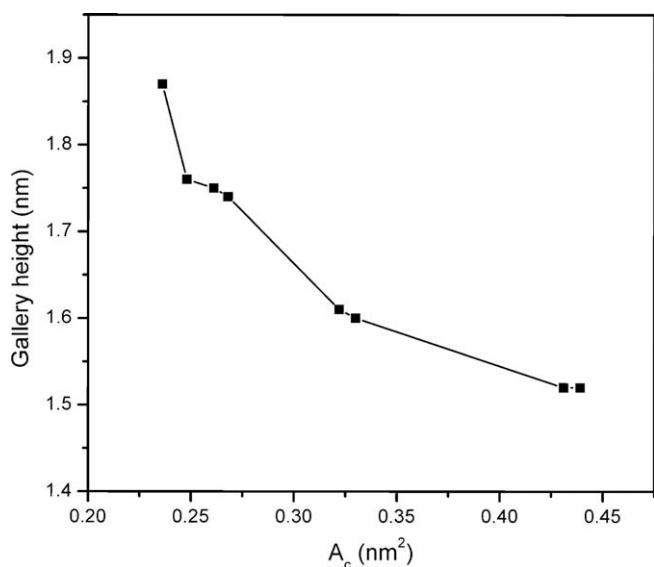
dark-field images, a uniform distribution of the Ti(IV)TA<sub>2</sub> complex throughout the disk-like slabs is clearly observed.

Fig. 4 shows the <sup>13</sup>C NMR spectra of gel-like and intercalated Ti(IV)TA<sub>2</sub>, which is expected to give information on the interaction between Ti(IV)TA<sub>2</sub> and the brucite-like layer. In the <sup>13</sup>C NMR spectrum of gel-like Ti(IV)TA<sub>2</sub> (Fig. 4a), one broad signal centered at 182.4 ppm, associated with the carboxyl carbon atoms, is observed. For pristine  $\iota$ -tartaric acid, this resonance is present at 176.5 ppm. The downshift from 176.5 to 182.4 ppm indicates the coordination of carbonyl oxygen to Ti center [35,36]. The resonance associated with alcoholic carbon shifts to 87.1 ppm and gets broad, which is present at 74.3 ppm for  $\iota$ -tartaric acid, revealing the coordination of alcoholic oxygen to Ti center. The non-disturbed signals at 171.6 ppm for carboxyl carbon and 72.5 ppm for alcoholic carbon result from the presence of un-coordinated carboxyl and alcoholic groups. The coordination of alkoxide with Ti is confirmed by the resonance at 65.5, 30.6, 19.0, and 13.1 ppm, which are attributed to the butoxy carbons. The butoxy groups result from the *trans*-esterification of Ti(O<sup>i</sup>Pr) with *n*-butanol as solvent [37,38]. The coordination of  $\iota$ -tartaric acid with Ti center in the Ti(IV)TA<sub>2</sub> complex prepared in this work thus resembles the Kagan-Medona structure [36]. The complex bears a hexacoordinate dimeric configuration, as shown in Fig. 5a. In this dimeric structure, each titanium atom is facially coordinated by one tartrate ligand through

the two diolate oxygen atoms. Another tartrate ligand links to the Ti center through one carbonyl oxygen and adjacent alcoholic oxygen, leaving the other alcoholic and carbonyl group un-coordinated. One alkoxy ligand is connected with titanium in *trans* location to the coordinated carbonyl oxygen. Two bridging diolate oxygen atoms binds the two titanium atoms together, producing a six-coordinate, pseudo-octahedral structure for each titanium center. The intercalation of Ti(IV)TA<sub>2</sub> into the LDH interlayer space causes better resolution and downfield shift of 182.4 and 87.1 resonances (Fig. 4b). The better resolution reflects the more definite and homogeneous chemical environment of the coordinated carboxylate and alcoholic carbons. The signal, originating from the carboxylic carbon coordinated with titanium, shifts from 182.4 to 184.3 ppm. The downshift is ascribed to the deprotonation of carboxylic groups that interact with brucite-like layer. The resonance at 172.1 ppm attributed to the un-coordinated carboxylic carbons is not disturbed by the intercalation. Due to the deprotonation of the two coordinated carboxyls in one complex molecule, the Ti(IV)TA<sub>2</sub> should be divalent anion. The strong electrostatic attraction between the brucite-like layer and the Ti(IV)TA<sub>2</sub> anions causes the decrease in electronic density of the coordinated alcoholic carbon, thus giving a shift from 87.1 to 89.0 ppm.

Using Materials Studio Program, the dimensions of Ti(IV)TA<sub>2</sub> molecule is estimated to be 1.00 × 1.29 × 1.08 nm. The interlayer space in each case (1.52–1.87 nm as observed by XRD patterns) of Mg/Al–Ti(IV)TA<sub>2</sub> LDHs exceeds the dimensions of one Ti(IV)TA<sub>2</sub> complex while is insufficient to the dimension of twofold Ti(IV)TA<sub>2</sub>. An interdigitated bilayer arrangement of Ti(IV)TA<sub>2</sub> in the interlayer gallery is proposed, with the coordinated carboxylate groups pointed to the brucite-like layer. The alkoxy groups tend to get adjacent through hydrophobic interaction with the alkoxy groups in another Ti(IV)TA<sub>2</sub> complex. From the dimensional size of Ti(IV)TA<sub>2</sub>, its cross-section area parallel to the ( $\vec{a}$ ,  $\vec{b}$ ) plane of brucite-like layer should be 1.39 nm<sup>2</sup> (1.29 × 1.08 nm). The area per charge of Ti(IV)TA<sub>2</sub> in this cross-section is 0.695 nm<sup>2</sup>, which is larger than  $A_c$  for all the brucite-like layers involved in this work. So, to compensate the layer charge, Ti(IV)TA<sub>2</sub> anions prefer to adopt a minimal projection on the brucite-like layer, giving a vertical interdigitated bilayer arrangement. Fig. 5b shows the schematic structure for Mg/Al–Ti(IV)TA<sub>2</sub> LDHs.

To investigate the arrangement of the interlayer Ti(IV)TA<sub>2</sub> anions along ( $\vec{a}$ ,  $\vec{b}$ ) plane and the interlacing degree of the adjacent Ti(IV)TA<sub>2</sub> anions, the area occupancy of Ti(IV)TA<sub>2</sub> anions ( $\chi$ ) compensating the charge of the brucite-like layer is defined.  $\chi = 0.695 \times O_c/A_c$ .  $O_c$  is the charge occupancy by interlayer Ti(IV)TA<sub>2</sub> anions.  $\chi = 1$ , when the summed cross-section area of interlayer Ti(IV)TA anions exactly equals the ( $\vec{a}$ ,  $\vec{b}$ ) plane area of single brucite-like layer. In that case, the interlayer Ti(IV)TA<sub>2</sub> anions are



**Fig. 2.** Dependence of interlayer spacing on  $A_c$  value for Mg/Al–Ti(IV)TA<sub>2</sub> LDHs.

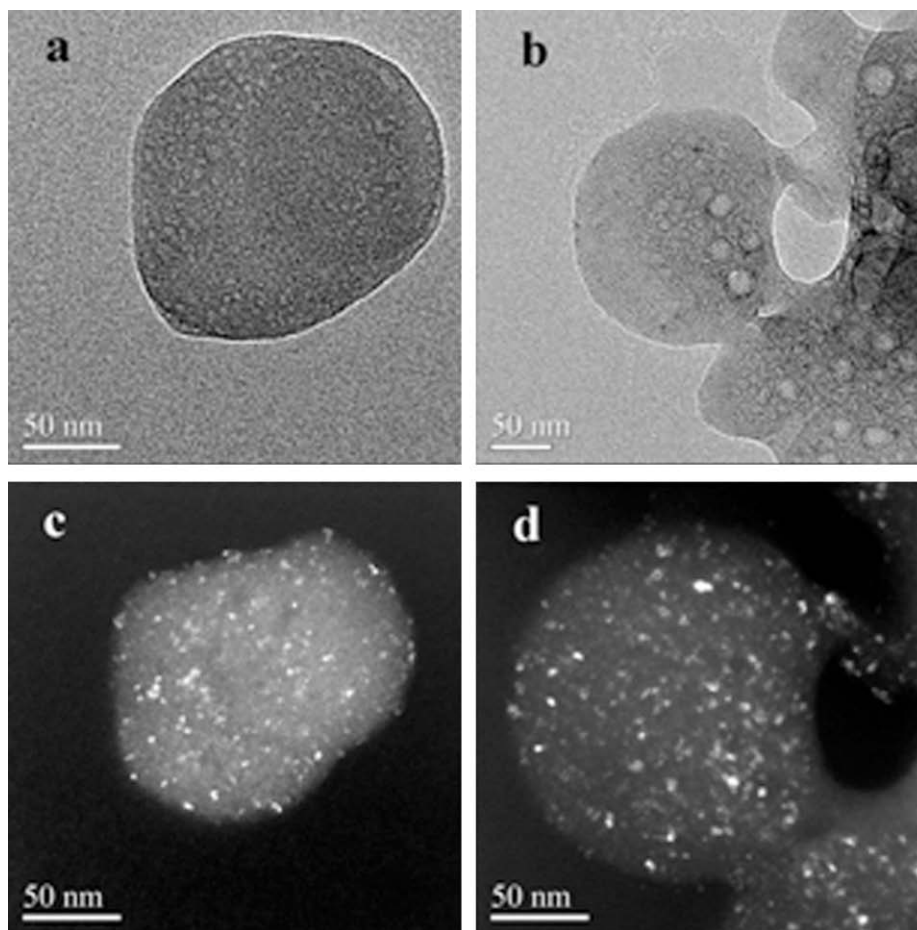


Fig. 3. Bright field (a and b) and dark-field (c and d) TEM images of  $Mg_{2.97}Al-Ti(IV)TA_2$  LDH.

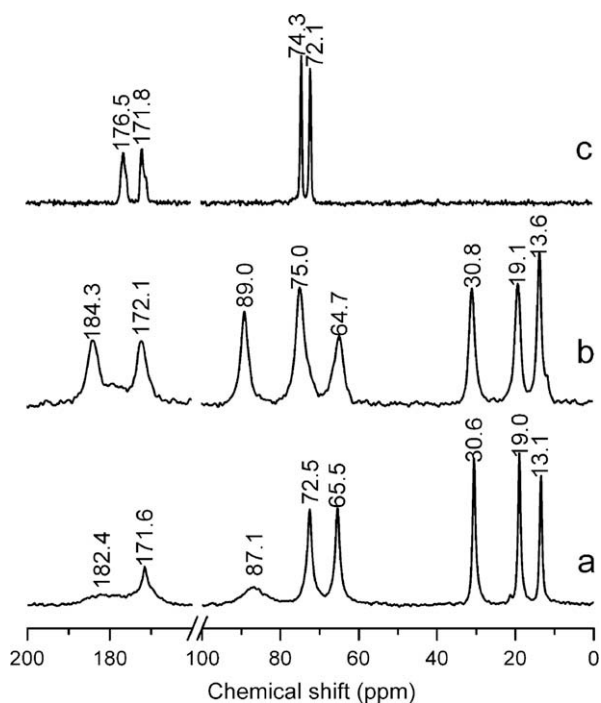


Fig. 4. Solid state  $^{13}C$  CP NMR spectra of (a)  $Ti(IV)TA_2$  complex, (b)  $Mg_{2.97}Al-Ti(IV)TA_2$  LDH, and (c) *L*-tartaric acid.

densely arranged one by one.  $\chi < 1$ , when the adjacent  $Ti(IV)TA_2$  anions are isolated in the interlayer.  $\chi > 1$ , when the adjacent  $Ti(IV)TA_2$  anions interlace in the direction parallel to the  $(\bar{a}, \bar{b})$  plane. The more the adjacent  $Ti(IV)TA_2$  anions are interlaced, the larger  $\chi$  is. It can be seen from Table 2 that, for the  $Mg/Al-Ti(IV)TA_2$  LDHs with similar interlayer spacing,  $\chi$  increases along with the ratio of interlayer  $Ti(IV)TA$  anions to co-existing tartrate. In other word, with more co-intercalated tartrate to compensate the charge of the brucite-like layer, the  $Ti(IV)TA_2$  anions in the interlayer space are arranged less densely. Therefore, the arrangement of interlayer  $Ti(IV)TA_2$  anions along the  $(\bar{a}, \bar{b})$  plane can be altered through the co-intercalation of small anions while the interlayer spacing is fixed.

### 3.3. Catalytic sulfoxidation

The  $Mg/Al-Ti(IV)TA_2$  LDHs were evaluated by the catalytic oxidation of pro-chiral methyl phenyl sulfide (MPS) using aqueous  $H_2O_2$  as oxidant. The results are shown in Tables 3–5.

The catalytic oxidation of MPS using  $Mg_{2.97}Al-Ti(IV)TA_2$  LDHs as catalysts was first performed in various solvents (Table 3). In DMF (Entry 1), the reaction affords methyl phenyl sulfoxide (MPSO) as the corresponding oxidation product with a selectivity of 95%, but the conversion is quite low even in 17 h. In acetone (Entry 2), the catalyst exhibits higher activity but no MPSO selectivity. The solvent with higher polarity (DMF) favors the MPSO selectivity, but disfavors the catalytic activity. Decreasing the polarity of the solvent promotes the activity but results in over-oxidation.  $CH_3CN$  and a  $MeOH/CH_2Cl_2$  mixture are then applied as solvents. In  $CH_3CN$

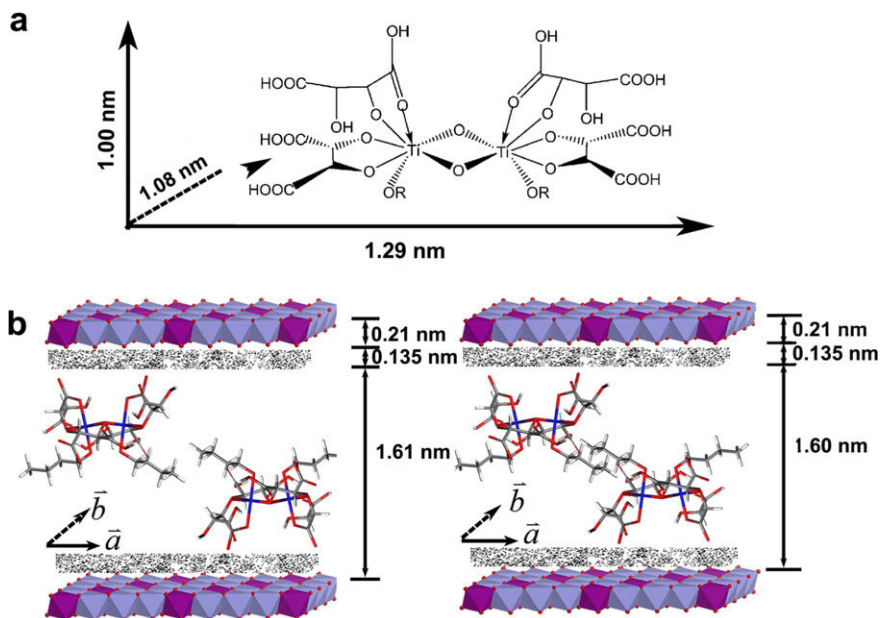


Fig. 5. Schematic structure of (a) Ti(IV)TA<sub>2</sub> and (b) Mg/Al-Ti(IV)TA<sub>2</sub> LDHs (C ●, H ○, O ●, Ti ●).

Table 2

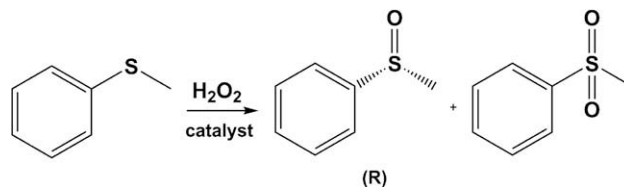
The dependence of the arrangement of the interlayer Ti(IV)TA<sub>2</sub> anions along ( $\bar{a}$ ,  $\bar{b}$ ) plane on the excess amount of L-tartaric acid.

Interlayer spacing (nm)	Ti(IV)TA <sub>2</sub> anions/tartrate in the interlayer	$\chi^a$	Proposed formula according to the chemical composition
1.52	2.44	1.09	[Mg <sub>0.81</sub> Al <sub>0.19</sub> (OH) <sub>2</sub> ] <sub>2</sub> [(Ti(IV)TA <sub>2</sub> ) <sub>0.06</sub> <sup>2-</sup> (C <sub>4</sub> H <sub>4</sub> O <sub>6</sub> ) <sub>0.03</sub> <sup>2-</sup> ]
1.52	0.96	0.43	[Mg <sub>0.81</sub> Al <sub>0.19</sub> (OH) <sub>2</sub> ] <sub>2</sub> [(Ti(IV)TA <sub>2</sub> ) <sub>0.03</sub> <sup>2-</sup> (C <sub>4</sub> H <sub>4</sub> O <sub>6</sub> ) <sub>0.03</sub> <sup>2-</sup> (CO <sub>3</sub> ) <sub>0.04</sub> <sup>2-</sup> ]
1.60	2.74	1.29	[Mg <sub>0.76</sub> Al <sub>0.24</sub> (OH) <sub>2</sub> ] <sub>2</sub> [(Ti(IV)TA <sub>2</sub> ) <sub>0.07</sub> <sup>2-</sup> (C <sub>4</sub> H <sub>4</sub> O <sub>6</sub> ) <sub>0.03</sub> <sup>2-</sup> (CO <sub>3</sub> ) <sub>0.02</sub> <sup>2-</sup> ]
1.61	0.74	0.67	[Mg <sub>0.75</sub> Al <sub>0.25</sub> (OH) <sub>2</sub> ] <sub>2</sub> [(Ti(IV)TA <sub>2</sub> ) <sub>0.04</sub> <sup>2-</sup> (C <sub>4</sub> H <sub>4</sub> O <sub>6</sub> ) <sub>0.05</sub> <sup>2-</sup> (CO <sub>3</sub> ) <sub>0.03</sub> <sup>2-</sup> ]
1.76	0.59	1.00	[Mg <sub>0.68</sub> Al <sub>0.32</sub> (OH) <sub>2</sub> ] <sub>2</sub> [(Ti(IV)TA <sub>2</sub> ) <sub>0.06</sub> <sup>2-</sup> (C <sub>4</sub> H <sub>4</sub> O <sub>6</sub> ) <sub>0.10</sub> <sup>2-</sup> (CO <sub>3</sub> ) <sub>0.01</sub> <sup>2-</sup> ]
1.75	0.27	0.45	[Mg <sub>0.69</sub> Al <sub>0.31</sub> (OH) <sub>2</sub> ] <sub>2</sub> [(Ti(IV)TA <sub>2</sub> ) <sub>0.03</sub> <sup>2-</sup> (C <sub>4</sub> H <sub>4</sub> O <sub>6</sub> ) <sub>0.10</sub> <sup>2-</sup> (CO <sub>3</sub> ) <sub>0.02</sub> <sup>2-</sup> ]

<sup>a</sup>  $\chi$  is denoted as the area occupancy of Ti(IV)TA<sub>2</sub> anions compensating the charge of the brucite-like layer.

Table 3

The oxidation of MPS catalyzed by Mg<sub>2.97</sub>Al-Ti(IV)TA<sub>2</sub> LDHs in different solvents



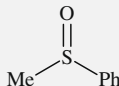
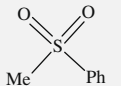
Entry <sup>a</sup>	Solvent	Ti/H <sub>2</sub> O <sub>2</sub> /substrate	Time (h)	Conv. (%) <sup>b</sup>	Product distribution (%)	
1	DMF	1/1.1/20	17	18	95	5
2	Acetone	1/1.1/20	1.5	24	–	100
3	CH <sub>3</sub> CN	1/1.1/20	2	32	77	23
4	CH <sub>3</sub> CN	1/1.1/20	5	53	69	31
5	CH <sub>2</sub> Cl <sub>2</sub>	1/1.1/20	2	–	–	–
6	MeOH/CH <sub>2</sub> Cl <sub>2</sub> v/v = 1/1)	1/1.1/20	2	18	93	7
7	MeOH/CH <sub>2</sub> Cl <sub>2</sub> v/v = 1/1)	1/1.1/20	9	51	89	11
8 <sup>c</sup>	MeOH/CH <sub>2</sub> Cl <sub>2</sub> v/v = 1/1)	0/1.1/20	9	10	100	0
9	CH <sub>3</sub> CN	1/1.1/20	9	68	60	40
10 <sup>c</sup>	CH <sub>3</sub> CN	0/1.1/20	9	4	100	0

<sup>a</sup> At 298 K.

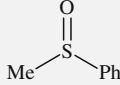
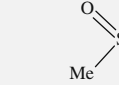
<sup>b</sup> Determined using GC-MS on a DB-5 column.

<sup>c</sup> Mg<sub>2.98</sub>Al-CO<sub>3</sub> LDH present in the reaction mixture, no Ti species introduced.

**Table 4**The oxidation of MPS catalyzed by Mg/Al–Ti(IV)TA<sub>2</sub> LDHs with different interlayer spacing.

Entry <sup>a</sup>	Catalyst	Interlayer spacing (nm) <sup>b</sup>	Solvent	Conv. (%)	Product distribution (%) <sup>c</sup>		ee (%) <sup>d</sup> (R)
							
1	Mg <sub>2.98</sub> Al–CO <sub>3</sub> LDH	0.28	MeOH/CH <sub>2</sub> Cl <sub>2</sub>	–	100	0	nd
				–	100	0	nd
2	Ti(IV)TA <sub>2</sub> complex	–	MeOH/CH <sub>2</sub> Cl <sub>2</sub>	100 <sup>e</sup>	96	4	5
			CH <sub>3</sub> CN	100 <sup>e</sup>	83	17	2
3	Ti(IV)TA <sub>2</sub> absorbed Mg <sub>2.98</sub> Al–CO <sub>3</sub> LDH	0.28	MeOH/CH <sub>2</sub> Cl <sub>2</sub>	20	87	13	10
			CH <sub>3</sub> CN	3	100	0	1
4	Mg <sub>4.37</sub> Al–Ti(IV)TA <sub>2</sub>	1.52	MeOH/CH <sub>2</sub> Cl <sub>2</sub>	44	92	8	36
			CH <sub>3</sub> CN	16	88	12	18
5	Mg <sub>2.97</sub> Al–Ti(IV)TA <sub>2</sub>	1.61	MeOH/CH <sub>2</sub> Cl <sub>2</sub>	29	97	3	48
			CH <sub>3</sub> CN	11	92	8	7
6	Mg <sub>2.21</sub> Al–Ti(IV)TA <sub>2</sub>	1.75	MeOH/CH <sub>2</sub> Cl <sub>2</sub>	32	93	7	23
			CH <sub>3</sub> CN	8	89	11	16
7	Mg <sub>1.94</sub> Al–Ti(IV)TA <sub>2</sub>	1.87	MeOH/CH <sub>2</sub> Cl <sub>2</sub>	27	97	3	23
			CH <sub>3</sub> CN	7	93	7	5
8	Mg <sub>3.10</sub> Al–Ti(IV)TA <sub>2</sub>	1.60	MeOH/CH <sub>2</sub> Cl <sub>2</sub>	53	94	6	46
			MeOH/CH <sub>2</sub> Cl <sub>2</sub>	47	96	4	26

<sup>a</sup> The reaction under the heterogeneous condition was processed for 9 h at 273 K.<sup>b</sup> The thickness of the clay layer 0.48 nm was subtracted from the basal spacing  $d_{003}$ .<sup>c</sup> Determined using GC–MS on a DB-5 column.<sup>d</sup> Determined by HPLC system with a chiral OB-H column (Daicel) and a *n*-hexane/*i*-propanol ( $v/v = 80/20$ , or  $v/v = 90/10$ ). “nd” is the abbreviation of “not determined”.<sup>e</sup> The 100% conversion was achieved less than 9 h.**Table 5**The oxidation of MPS catalyzed by Mg<sub>3.05</sub>Al–Ti(IV)TA LDH.

Entry <sup>a</sup>	Solvent	Time (h)	Conv. (%)	Product distribution (%) <sup>b</sup>		ee (%) <sup>c</sup> (R)
						
Ti(IV)TA complex	MeOH/CH <sub>2</sub> Cl <sub>2</sub>	1	100	90	10	8
Mg <sub>3.05</sub> Al–Ti(IV)TA	MeOH/CH <sub>2</sub> Cl <sub>2</sub>	9	34	90	10	24
Ti(IV)TA complex	CH <sub>3</sub> CN	5	99	73	27	1
Mg <sub>3.05</sub> Al–Ti(IV)TA	CH <sub>3</sub> CN	9	26	80	20	12

<sup>a</sup> At 273 K.<sup>b</sup> Determined using GC–MS on a DB-5 column.<sup>c</sup> Determined by HPLC system with a chiral OB-H column (Daicel) and a *n*-hexane/*i*-propanol ( $v/v = 80/20$ ).

(Entry 3), the reaction turns out a conversion of 32% and a MPSO selectivity of 77% in 2 h. Using the mixture ( $v/v = 1/1$ ) of polar MeOH and apolar CH<sub>2</sub>Cl<sub>2</sub> as solvent (Entry 6), the reaction turns out a conversion of 18% in 2 h and a MPSO selectivity of 93%. The introduction of MeOH improves the catalytic activity (in comparison with Entry 5), because MeOH facilitates the compatibility to aqueous H<sub>2</sub>O<sub>2</sub>. In 9 h, the conversion rises to 51% while no marked reduction has occurred to the MPSO selectivity (Entry 7). With a similar conversion, MeOH/CH<sub>2</sub>Cl<sub>2</sub> produces higher MPSO selectivity (Entry 7) than CH<sub>3</sub>CN (Entry 4). In both CH<sub>3</sub>CN and MeOH/CH<sub>2</sub>Cl<sub>2</sub> solvents, Mg<sub>2.97</sub>Al–Ti(IV)TA<sub>2</sub> LDHs (Entries 7 and 9) gives much higher conversion than Mg<sub>2.98</sub>Al–CO<sub>3</sub> LDH (Entries 8 and 10), demonstrating the major contribution of intercalated Ti(IV)–TA<sub>2</sub> to the catalytic activity.

The asymmetric sulfoxidation of MPS was carried out in CH<sub>3</sub>CN and MeOH/CH<sub>2</sub>Cl<sub>2</sub> ( $v/v = 1/1$ ) at 273 K, with the input ratio of substrate/Ti/H<sub>2</sub>O<sub>2</sub> fixed at 20/1/1.1. A blank reaction, with the presence of Mg<sub>2.98</sub>Al–CO<sub>3</sub> LDH, was first performed. As shown in Table 4, negligible conversion has been accomplished in 9 h in either MeOH/CH<sub>2</sub>Cl<sub>2</sub> or CH<sub>3</sub>CN. The Payne reagent [39] formed by CH<sub>3</sub>CN and H<sub>2</sub>O<sub>2</sub> contributes little to the oxidation. Ti(IV)TA<sub>2</sub> complex in homogenous system gives complete conversion of MPS but disappointing enantioselectivities in both solvents (8% ee in MeOH/

CH<sub>2</sub>Cl<sub>2</sub> and 2% ee in CH<sub>3</sub>CN). The heterogeneous catalytic oxidation in MeOH/CH<sub>2</sub>Cl<sub>2</sub> all exhibit improved enantioselectivity. The MPSO was determined as *R* absolute configuration using the circular dichroism (CD) spectroscopy, showing a positive/negative sequence in the sign of its Cotton effect on moving from longer to shorter wavelengths [40]. The Cotton effect signal is strong for the product using Mg<sub>2.97</sub>Al Ti(IV)TA<sub>2</sub> LDHs as heterogeneous catalyst, while it is much weaker for the product of homogeneously catalytic reaction. Only case improvement of enantioselectivity is observed in CH<sub>3</sub>CN. The difference in the enantioselectivity could attribute to the solvent effects. But it can be further found in CH<sub>3</sub>CN that the enantioselectivity induced by Mg/Al–Ti(IV)TA<sub>2</sub> LDHs is similar to that induced by Ti(IV)TA<sub>2</sub> absorbed Mg<sub>2.98</sub>Al–LDH. However, in MeOH/CH<sub>2</sub>Cl<sub>2</sub> the enantioselectivity induced by Mg/Al–Ti(IV)TA<sub>2</sub> LDHs is greater than that induced by Ti(IV)TA<sub>2</sub> absorbed Mg<sub>2.98</sub>Al–LDH. Does the ee diversity in MeOH/CH<sub>2</sub>Cl<sub>2</sub> and CH<sub>3</sub>CN involve the position where the catalysis takes place? The catalytic oxidation Mg/Al–Ti(IV)TA<sub>2</sub> LDHs took place on the exterior surface or at the slab edges of the intercalated phase in CH<sub>3</sub>CN, while in the interlayer regions in MeOH/CH<sub>2</sub>Cl<sub>2</sub>? The conversion on Mg/Al–Ti(IV)TA<sub>2</sub> LDHs in CH<sub>3</sub>CN, which is at the same level as that catalyzed by Ti(IV)TA<sub>2</sub> absorbed Mg<sub>2.98</sub>Al–LDH, seems consistent with the above assumption. The interlayer Ti center is less accessi-

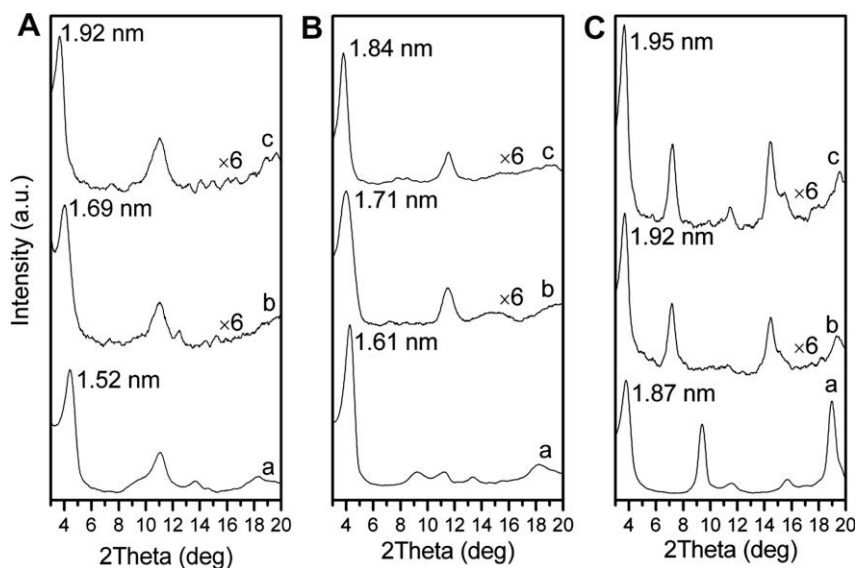


Fig. 6. XRD patterns of (a) original and swollen Mg/Al-Ti(IV)TA<sub>2</sub> LDHs in (b) CH<sub>3</sub>CN and (c) MeOH/CH<sub>2</sub>Cl<sub>2</sub>.

ble to the reactant, resulting in a low conversion. However, in MeOH/CH<sub>2</sub>Cl<sub>2</sub>, the conversions on Mg/Al-Ti(IV)TA<sub>2</sub> LDHs are evidently higher than on Ti(IV)TA<sub>2</sub> absorbed Mg<sub>2.98</sub>Al-LDH.

To elucidate the differences between the catalysis in CH<sub>3</sub>CN and MeOH/CH<sub>2</sub>Cl<sub>2</sub>, the interlayer swelling of Mg/Al-Ti(IV)TA<sub>2</sub> LDHs was carried out. Mg/Al-Ti(IV)TA<sub>2</sub> LDHs was suspended in the solvent dissolving MPS. After 1 h stirring, the solid was removed from the suspension by centrifugation and directly exposed to XRD characterization. The XRD patterns are shown in Fig. 6. The observed shift of the basal reflections to small 2θ degree confirms the increase in the interlayer spacing ( $\Delta h$ ) of Mg/Al-Ti(IV)TA<sub>2</sub> LDHs. In MeOH/CH<sub>2</sub>Cl<sub>2</sub>, the Mg/Al-Ti(IV)TA<sub>2</sub> LDH with an original interlayer spacing of 1.52, 1.61, and 1.87 nm displays an  $\Delta h$  of 0.40, 0.23, and 0.08 nm, respectively. More obvious interlayer swelling means that more reactants are accommodated in the interlayer regions, allowing catalytic reactions to occur on the interlayer active Ti center. Evident ee increment (Table 4) is thus observed, from 10% on Ti(IV)TA<sub>2</sub> absorbed Mg<sub>2.98</sub>Al-LDH (Entry 3) to 36%, 48% or 23% on Mg/Al-Ti(IV)TA<sub>2</sub> LDH (Entries 4–7). In CH<sub>3</sub>CN, the Mg/Al-Ti(IV)TA<sub>2</sub> LDH with an original interlayer spacing of 1.52, 1.61, and 1.87 nm displays an  $\Delta h$  of 0.17, 0.10, and 0.05 nm respectively, which is smaller than that in MeOH/CH<sub>2</sub>Cl<sub>2</sub> in each case. The biggest increment of ee (18%) is also observed on the LDH with the biggest  $\Delta h$  (Entry 4). The inferior  $\Delta h$  accounts for the less increment of the enantioselectivity observed in CH<sub>3</sub>CN.

The swelling experiments indicate that  $\Delta h$  decreases with the increase in original interlayer spacing. It is not difficult to understand because the interaction between the brucite-like layer and interlayer anions gets stronger with the decrease in  $A_c$ . For the catalysis taking place in the interlayer regions, the ee value generally decreases with the increase in the original interlayer spacing, consistent with the swelling behavior (Entries 5–7). But the ee on Mg<sub>4.37</sub>Al-Ti(IV)TA<sub>2</sub> LDH (Entry 4), which has the largest interlayer expansion, is not the highest one as expected. This can attribute to the over-enlarged interlayer spacing (1.92 nm), which has less steric constraint.

Increasing  $\chi$  value under a similar interlayer spacing (Entries 5 and 8, Entries 6 and 9), the ee value shows little change, but the conversion increased. This result implies that the distance of adjacent Ti(IV)TA<sub>2</sub> anions along ( $\bar{a}$ ,  $\bar{b}$ ) plane affects the contact of reactants to the active Ti center, but has little influence on the enantioselectivity.

The ion-exchange of Mg<sub>2.98</sub>Al-CO<sub>3</sub> LDH with Ti(IV)TA complex has also been carried out with the input ratio of L-tartaric acid/Ti = 1, exactly the stoichiometric ratio of Sharpless coordination structure. The (0 0 3) and (0 0 6) reflections shift to  $2\theta = 4.6^\circ$  and  $9.1^\circ$ , as can be seen from Fig. 7a, giving a basal spacing of 1.92 nm and an interlayer spacing of 1.44 nm. The resulting Mg<sub>3.05</sub>Al-Ti(IV)TA LDH has also been used as a catalyst in the sulfoxidation (Table 5). In CH<sub>3</sub>CN, the interlayer expansion is observed as 0.05 nm, giving a 12% ee. In MeOH/CH<sub>2</sub>Cl<sub>2</sub>, a 24% ee is achieved, in accord with a larger interlayer expansion ( $\Delta h = 0.35$  nm).

Therefore, the heterogeneous catalysis restricted in the bidimensional space induces asymmetric selectivity. The spatial confinement is resulted from the flexible interlayer spacing tuned by the area unit charge of the brucite-like layer.

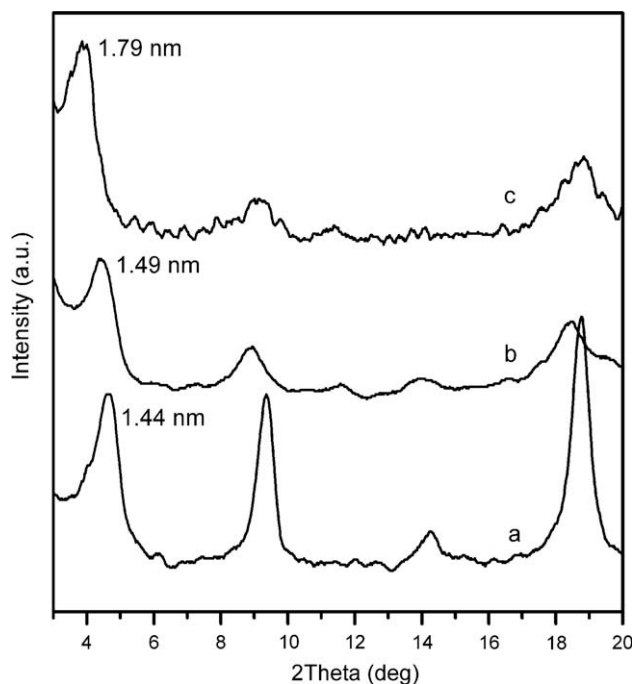


Fig. 7. XRD patterns of (a) original and swollen Mg/Al-Ti(IV)TA LDH in (b) CH<sub>3</sub>CN and (c) MeOH/CH<sub>2</sub>Cl<sub>2</sub>.



#### 4. Conclusions

In conclusion, Mg/Al-LDHs intercalated with Kagan-Medona and Sharpless titanium tartrate complexes have been prepared and applied in the asymmetric catalytic sulfoxidation. The interlayer spacing of Ti(IV)TA<sub>m</sub> LDHs is varied in the range of 1.44 and 1.87 nm by tuning the area unit charge of the brucite-like layer. The Mg/Al–Ti(IV)TA<sub>m</sub> LDHs with flexible interlayer spaces brought in the increment of enantiomeric excess compared with the homogeneous counterpart. The steric confinement of the bidimensional space is considered to play an important role in the enantioselectivity enhancement.

#### Acknowledgments

The authors are grateful to the financial support from NSFC and “973” Program (2009CB939802).

#### Appendix A. Supplementary material

Supplementary data associated with this article can be found, in the online version, at [doi:10.1016/j.jcat.2010.02.006](https://doi.org/10.1016/j.jcat.2010.02.006).

#### References

- [1] D.C. Bailey, S.H. Langer, *Chem. Rev.* 81 (1981) 109.
- [2] M.M. Paul, J.H. Graham, *Chem. Soc. Rev.* 33 (2004) 108.
- [3] Q.-H. Xia, H.-Q. Ge, C.-P. Ye, Z.-M. Liu, K.-X. Su, *Chem. Rev.* 105 (2005) 1603.
- [4] T. Katsuki, K.B. Sharpless, *J. Am. Chem. Soc.* 102 (1980) 5974.
- [5] M.J. Farrell, M. Alexis, M. Trecarten, *Nouv. J. Chim.* 7 (1983) 449.
- [6] L. Canali, J.K. Karjalainen, D.C. Sherrington, O. Hormi, *Chem. Commun.* (1997) 123.
- [7] B.M. Choudary, V.L.K. Valli, A.D. Prasad, *J. Chem. Soc. Chem. Commun.* (1990) 1186.
- [8] S. Xiang, Y.-L. Zhang, Q. Xin, C. Li, *Angew. Chem. Int. Ed.* 41 (2002) 821.
- [9] J.M. Notestein, A. Katz, *Chem. Eur. J.* 12 (2006) 3954.
- [10] J.M. Fraile, J.I. García, J.A. Mayoral, M. Roldán, *Org. Lett.* 9 (2007) 731.
- [11] C. Li, H. Zhang, D. Jiang, Q. Yang, *Chem. Commun.* (2007) 547.
- [12] A. Corma, H. García, G. Sastre, P.M. Viruela, *J. Phys. Chem. B* 101 (1997) 4575.
- [13] M.K. Kidder, P.F. Britt, Z. Zhang, S. Dai, E.W. Hagaman, A.L. Chaffee, A.C. Buchanan, *J. Am. Chem. Soc.* 127 (2005) 6353.
- [14] F. Goettmanna, C. Sanchez, *J. Mater. Chem.* 17 (2007) 24.
- [15] H.-Q. Yang, L. Zhang, L. Zhong, Q.-H. Yang, C. Li, *Angew. Chem. Int. Ed.* 46 (2007) 6861.
- [16] R. Raja, J.M. Thomas, M.D. Jones, B.F.G. Johnson, D.E.W. Vaughan, *J. Am. Chem. Soc.* 125 (2003) 14982.
- [17] M.D. Jones, R. Raja, J.M. Thomas, B.F.G. Johnson, D.W. Lewis, J. Rouzard, K.D.M. Harris, *Angew. Chem. Int. Ed.* 42 (2003) 4326.
- [18] H.-D. Zhang, S. Xiang, C. Li, *Chem. Commun.* (2005) 1209.
- [19] X.-G. Zhou, X.-Q. Yu, J.-S. Haung, S.-G. Li, L.-S. Li, C.-M. Che, *Chem. Commun.* (1999) 1789.
- [20] S. Xiang, Y. Zhang, Q. Xin, C. Li, *Chem. Commun.* (2002) 2696.
- [21] V. Caps, I. Paraskevas, S.-C. Tsang, *Chem. Commun.* (2005) 1781.
- [22] B.F.G. Johnson, S.A. Raynor, D.S. Shephard, T. Mashmeyer, J.M. Thomas, G. Sankar, S. Bromley, R. Oldroyd, L. Gladden, M.D. Mantle, *Chem. Commun.* (1999) 1167.
- [23] D.G. Evans, R.C.T. Slade, *Struct. Bond.* 119 (2006) 161.
- [24] A.I. Khan, D. O'Hare, *J. Mater. Chem.* 12 (2002) 3191.
- [25] D. Carriazo, C. Domingo, C. Martín, V. Rives, *Inorg. Chem.* 45 (2006) 1243.
- [26] V. Rives, M.A. Ulibarri, *Coord. Chem. Rev.* 181 (1999) 61.
- [27] S. Bhattacharjee, J.A. Anderson, *Chem. Commun.* (2004) 554.
- [28] B.M. Choudary, N.S. Chowdari, M.L. Kantam, K.V. Raghavan, *J. Am. Chem. Soc.* 123 (2001) 9220.
- [29] M. Halma, K.A.D.F. Castro, C. Taviot-Gueho, V. Prévot, C. Forano, F. Wypych, S. Nakagaki, *J. Catal.* 257 (2008) 233.
- [30] B.M. Choudary, S. Madhi, N.S. Chowdari, M.L. Kantam, B. Sreedhar, *J. Am. Chem. Soc.* 124 (2002) 14127.
- [31] Y. Zhao, F. Li, R. Zhang, D.G. Evans, X. Duan, *Chem. Mater.* 14 (2002) 4286.
- [32] F. Leroux, M. Adachi-Pagano, M. d Intissar, S. Chauvière, C. Forano, J.P. Besse, *J. Mater. Chem.* 11 (2001) 105.
- [33] D.G. Evans, R.C.T. Slade, *Struct. Bond.* 119 (2006) 15.
- [34] D.G. Evans, R.C.T. Slade, *Struct. Bond.* 119 (2006) 10.
- [35] P.G. Potvin, S. Bianchet, *J. Org. Chem.* 57 (1992) 6629.
- [36] P.G. Potvin, B.G. Fieldhouse, *Tetrahedron-Asymmetr.* 10 (1999) 1661.
- [37] S.S. Woodard, M.G. Finn, K.B. Sharpless, *J. Am. Chem. Soc.* 113 (1991) 106.
- [38] M.G. Finn, K.B. Sharpless, *J. Am. Chem. Soc.* 113 (1991) 113.
- [39] W.C. Frank, *Tetrahedron-Asymmetr.* 9 (1998) 3745.
- [40] C. Rosini, M.I. Donnoli, S. Superchi, *Chem. Eur. J.* 7 (2001) 72.